Journal of Systems Engineering and Electronics
Vol. 34, No. 5, October 2023, pp.1147 – 1157

Deep convolutional neural network for meteorology target detection in airborne weather radar images

YU Chaopeng[1,†], XIONG Wei[1,†,*], LI Xiaoqing[1], and DONG Lei[2]

1. Aviation Industry Corporation of China Leihua Electronic Technology Institute, Wuxi 214063, China;
2. Key Laboratory of Civil Aircraft Airworthiness Technology, Civil Aviation University of China, Tianjin 300300, China

Abstract: Considering the problem that the scattering echo images of airborne Doppler weather radar are often reduced by ground clutters, the accuracy and confidence of meteorology target detection are reduced. In this paper, a deep convolutional neural network (DCNN) is proposed for meteorology target detection and ground clutter suppression with a large collection of airborne weather radar images as network input. For each weather radar image, the corresponding digital elevation model (DEM) image is extracted on basis of the radar antenna scanning parameters and plane position, and is further fed to the network as a supplement for ground clutter suppression. The features of actual meteorology targets are learned in each bottleneck module of the proposed network and convolved into deeper iterations in the forward propagation process. Then the network parameters are updated by the back propagation iteration of the training error. Experimental results on the real measured images show that our proposed DCNN outperforms the counterparts in terms of six evaluation factors. Meanwhile, the network outputs are in good agreement with the expected meteorology detection results (labels). It is demonstrated that the proposed network would have a promising meteorology observation application with minimal effort on network variables or parameter changes.

Keywords: meteorology target detection, ground clutter suppression, weather radar images, convolutional neural network (CNN).

DOI: 10.23919/JSEE.2023.000142

1. Introduction

The capability of microwaves to penetrate clouds and rain has placed the weather radar in an unchallenged position for remotely surveying the atmosphere. The Doppler weather radar is currently the primary tool that can measure the scattering echo powers and radial velocities, both in clear air and inside heavy rainfall regions veiled by clouds. It is claimed that Doppler weather radars have been the most important sensors for atmosphere surveillance [1−5]. Unlike ground-based weather radars, the working mode of airborne weather radar is generally downward-looking or head-up looking. For the airborne weather radar, the expected meteorological echo is often severely affected by various ground clutters, which are difficult to suppress effectively, due to the relatively moving status, wide clutter spectrum and strong clutter power. Thus, it is difficult to directly analyze the radar echo, detect actual meteorology targets and further warn meteorology hazardous areas. The flying-safety of planes would be confronted with dangerous meteorology threats.

When the radar beam contacts the ground, the received echo includes the meteorological echo and the ground clutters. The ground clutters are generated by mountains, hills, and forests in the same radar beam of the meteorological echo. Unfortunately, the ground clutter power is generally stronger than that of actual meteorology targets and the ground clutter spectrum is also wider. Considering the problem that the scattering echo images of airborne Doppler meteorological radar are severely affected by ground clutters, such as non-rainfall, the accuracy and confidence of the refined meteorology target detection are reduced. Thus, it is vital to suppress the ground clutters before the meteorology target detection and classification [5].

Recently, the deep convolutional neural network (DCNN) as the state-of-the-art machine learning model has the ability of automatically extracting sample features and has been successfully applied in computer vision [6−10], radar automatic target recognition [11−15] and climate observation fields [1−5,16−21]. In view of

Manuscript received July 01, 2022.
*Corresponding author.
†Co-first authors.
This work was supported by the China Ministry of Industry and Information Technology Foundation and Aeronautical Science Foundation of China (ASFC-201920007002), the National Key Research and Development Plan (2021YFB1600603), and the Open Fund of Key Laboratory of Civil Aircraft Airworthiness Technology, Civil Aviation University of China.

deep learning (DL), meteorology target detection and ground clutter suppression in weather radar images are similar to the image semantic segmentation, where the network input is a multichannel image and the output is assigned to every pixel. Inspired by the DL-based image segmentation approaches [9,22−26], a semantic segmentation-based DCNN is proposed for the meteorology target detection and ground clutter suppression in weather radar images in this paper. The digital elevation model (DEM) images are also employed as a supplement to the weather radar echo images and fed to the DCNN together for training. A DEM image is composed of a grid of pixels spaced at regular intervals, with the pixel value representing elevation at that point. In each regular interval, the geographic location and height of terrain can be calculated and terrain characteristics in different intervals would vary. In this work, we first estimate whether the weather radar beam contacts the ground. When the beam contacts the ground, the horizontal ranges of the contactors apart from the airborne weather radar are then calculated. After that, the DEM image of ground clutter regions can be obtained and is further fed to the proposed DCNN for ground clutter learning. To the best of the authors' knowledge, this is the first work that employs DCNN and DEM images as a supplement to weather radar images to suppress the ground clutters in airborne weather radar images.

The outline of the paper is as follows. In Section 2, the related approaches to meteorology detection and precipitation are reviewed and presented. In Section 3, the methodology based on a DCNN is described in detail. The experimental design and evaluation result analysis are described in Section 4. Finally, Section 5 concludes the paper and discusses the future work.

2. Related work

The airborne weather radar images often contain the information about actual meteorology, ground clutters, and noise. For the challenging task of meteorology target detection, warning, and forecasting, it has been problematic to effectively extract and learn the features of meteorology targets and ground clutters from multisource raw data, due to a lack of computation and meteorology observation data. In recent years, advancements in DL techniques [22−29] and graphics processing units (GPU) make it possible. Meanwhile, severe weather detection is a typical research domain that uses weather radar images as the primary input data. Due to the end-to-end abstract ability and multilayered feature representation, DL methods are typically expected to perform better than the shallow machine learning methods, such as the features-based support vector machine (SVM). As a traditional DL method, convolutional neural network (CNN) has been the state-of-the-art solution for semantic segmentation [1,2,11], so it is reasonable to apply the similar neural networks for precipitation prediction and ground clutter suppression in weather radar images.

The traditional meteorology detection and prediction methods mainly rely on algorithms that detect and extrapolate radar echo observations or expert systems on basis of the predefined rules and thresholds [1−3]. Much work has been paid to the prior knowledge-based feature extraction and threshold tuning, which makes these algorithms difficult to be directly applied in varying scenarios due to the poor adaptability. In contrast, the CNN-based methods directly start from raw radar data and compute a layer-wise transformation of each representation, producing abstract levels with increasingly improved feature representation. By employing a series of these transformations, thus complex feature representations can be learned automatically without the use of handcraft feature engineering [3−5]. Expected detection and classification results can be obtained without threshold tuning. It is demonstrated that the CNN-based radar meteorology detection has a promising application.

Wang et al. [1] proposed a CNN algorithm to firstly extract useful features from the polarimetric measurements of dual-polarization Doppler weather radar, then the extracted features were classified by Softmax classifier, and the precipitation particles were finally divided into rain, snow, ice crystals, hail, and other categories. The experimental results were in good agreement with the ground observation data. Han et al. [2] examined an end-to-end DL nowcasting method using three-dimensional (3D) radar images and reanalysis data, where the nowcasting problem was transformed into a classification problem. Guang et al. [3] discussed a deep recurrent neural network model for predicting image sequences of weather radars and proposed a new adaptive loss to train the model. Meanwhile, image discriminators were designed to ensure the continuity of sequences and visual quality of images. Gurung et al. [4] employed a DCNN to detect hailstorm events in a large collection of radar images, where the effectiveness of training and classification was discussed using different activation functions and different pooling methods in network layers. Evaluation results of the proposed DCNN showed high classification accuracy in comparison with existing hailstorm detection approaches. Considering the problem that the scattering echo image of the new generation Doppler meteorological radar is reduced by noise, Yang et al. [5] proposed a DCNN-based method for semantic segmentation of meteorological radar noise image, and experimental results showed that the proposed method had better denoising effects on meteorological radar images than the

optical flow method and the fully convolutional networks (FCN).

Inspired by [1−5], the meteorology target detection and ground clutter suppression problem in weather radar images is similarly transformed into an image semantic segmentation problem in this paper. We present a DCNN-based method to carry out meteorology target detection, where the weather radar images and DEM images are all employed as multi-channel input to feed to the DCNN together. Operationally produced airborne weather radar data from different regions and different weather conditions is used to train the proposed DCNN and to evaluate its performance. Experimental results on the real measured images demonstrate that our method has the state-of-the-art performances.

3. Methodology

As shown in Fig. 1, we give an overview of the proposed end-to-end DL approach for meteorology target detection and ground clutter suppression of weather radar. The meteorology target detection is considered as a target classification problem in images. In the data preprocessing, the radar echo images are first transferred to the reflectivity factor (RF) images. Meanwhile the corresponding DEM images of the radar beam scanning regions are extracted from a DEM dataset. Then these images are fed as the multichannel input to our proposed CNN model for training. Finally, the trained model is employed to detect actual meteorology targets and also suppress ground clutters at the same time.

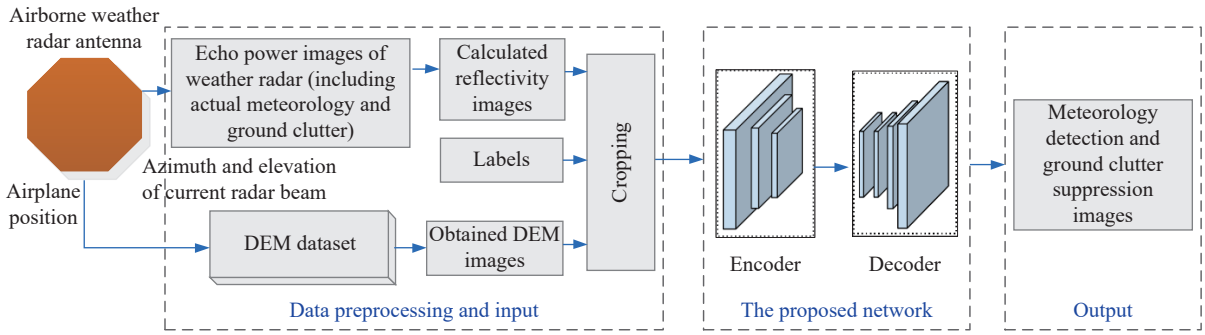

Fig. 1 Flowchart of our proposed DL approach for meteorology detection and ground clutter suppression

3.1 Preprocessing

Often, the Doppler weather radar transmits waves to obtain the RF [1], which is defined as

$$Z = \int_0^{\eta_{\max}} N(\eta)\cdot\bar{\eta}^6 \mathrm{d}\eta \tag{1}$$

where η is the precipitation particle diameter, $\eta_{\max}$ denotes the maximum diameter, $\bar{\eta}$ refers to the projection of η in horizontal or vertical polarization direction, and $N(\cdot)$ is the drop distribution function of precipitation particles. When $\bar{\eta}$ is the horizontal projection, Z is the horizontal RF. When $\bar{\eta}$ is the vertical projection, Z denotes the vertical RF. It is seen that RF is related with the particle diameter, drop distribution, and dielectric constant. For the rainfall, the effect of particle diameter on RF is greater, and the larger particle size produces the larger RF [1]. In addition, for hail, raindrops, and other different types of precipitation particles, the RF is also affected by the dielectric constant. Therefore, we can infer the meteorology target type based on the difference in RF characteristics.

3.1.1 Meteorology RF calculation

Consider that an airborne Doppler weather radar system is equipped with a non-uniform array and emits a distinct waveform to a meteorology region. The azimuth and elevation angles of radar beam are denoted as θ and φ, respectively. When the radar transmitted power is P_t, the transmitted and received gains are denoted as G_t, G_r, and the radical range between meteorology target and weather radar is represented as R, we can calculate the meteorology RF Z [29] based on the received echo power P_r by

$$Z = \frac{1\,024\ln 2}{\pi^3}\cdot\frac{R^2\lambda^2 L_a L_s}{P_t G_t G_r \theta\varphi c\tau}\cdot\frac{P_r}{\xi|K|^2} \tag{2}$$

where λ is the wavelength, L_a is the round-trip attenuation factor of radar waveform, $\xi \leqslant 1$ denotes the filling factor, c is the speed of light, L_s is the system loss, $K = \dfrac{m^2-1}{m^2+2}$ is a constant calculated by the complex refractive index m of meteorology. We set the water at 0°C−20°C as an example, $|K|^2 = 0.93$. Meanwhile, for ice at all temperatures, $|K|^2 = 0.197$. When the beam is filled with meteorology scatters, $\xi = 1$, otherwise $\xi < 1$. Thus, we can get the RF distribution images from the radar echo images based on (2), which can show the reflectivity intensity of meteorology target.

To visually display the meteorology caution areas for pilots, the RF distribution images are often normalized and marked with different colors. Fig. 2 is a typical normalized RF image, where the red, yellow, and green represent the large, middle and small RFs, respectively. Due to the downward-looking or head-up looking of airborne weather radar, the expected meteorological echo is often severely affected by various ground clutters. It is demonstrated that Fig. 2 can not only show the RF distribution of precipitation particles in atmosphere, but also provide the RFs of ground clutters. Thus it is vital to effectively suppress ground clutters for the meteorology target detection and further meteorology caution area warning.

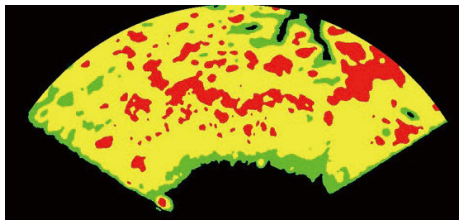

Fig. 2 A calculated RF image

3.1.2 DEM image obtainment

In this work, the DEM images are employed to train the network for ground clutter feature learning and distinguishing. As shown in Fig. 3, we first calculate the scanning line-of-sight (SLOS) of current radar beam with azimuth angle θ and elevation angle φ, based on the longitude, latitude, and height of carrier. More details can be found in [30,31].

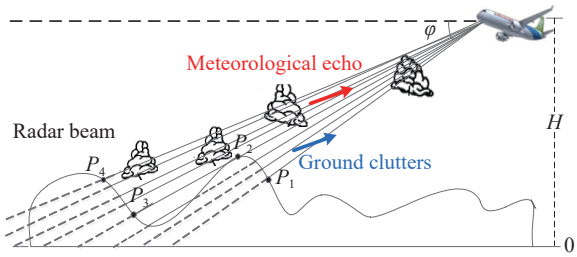

Fig. 3 Visible region of airborne weather radar beam

We set the current radar beam in Fig. 3 as an example. It is shown that the region between P_1 and P_2, and the region between P_3 and P_4 are radiated by the radar beam, while the region between P_2 and P_3 is shaded. Meanwhile, it is noticed that the extracted DEM data must match the radar beam radiation regions. Therefore, the corresponding shaded regions and radiated regions are assigned 0 and 1, respectively. Then, the extracted DEM data becomes a binary image. A typical DEM image corresponding to Fig. 2 is depicted as follows, where the employed DEM dataset is the NASA open earth data and can be obtained from https://search.earthdata. nasa.gov/.

3.1.3 Labeling

In the semantic segmentation field, the corresponding labels of input images are often artificial-made on basis of the prior knowledge. Unfortunately, for the meteorology target, it is difficult to accurately label, even for the meteorology professionals. Herein, we select the final meteorology detection results of actual airborne weather radar as the labels, which are obtained followed by a series of processing, such as the classical meteorology target detection, DEM-based clutter suppression, color quantization, and so on. Fig. 5 is the airborne weather radar's final output result of Fig. 2 and is selected as the label.

3.1.4 Cropping images

It is well known that many input samples are necessary to fed to a CNN model for effective training. However, the actually measured RF images and matched DEM images of the same airborne weather radar are usually not enough. Similar to [4], the trick of cropping image is adopted to increase the input images and also decrease the network complexity. Herein we set the height and width of cropped window as 160 pixels and 180 pixels. To make the cropping and following restituting processing sufficient, we slide the cropping window in original images by the step of 80 pixels along the width direction and 90 pixels along the height direction, respectively. Then an original image can be divided into 13 cropped patches. We set the cropped images of Fig. 2, Fig. 4, and Fig. 5 as examples, which are shown in Fig. 6.

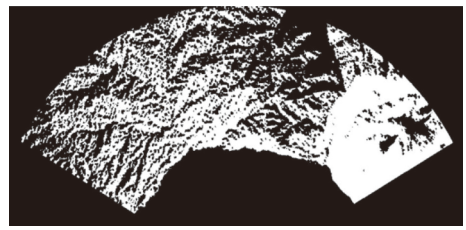

Fig. 4 A typical DEM image corresponding to Fig. 2

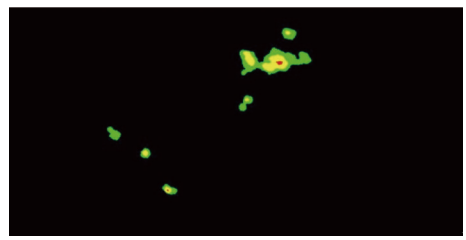

Fig. 5 The label of Fig. 2

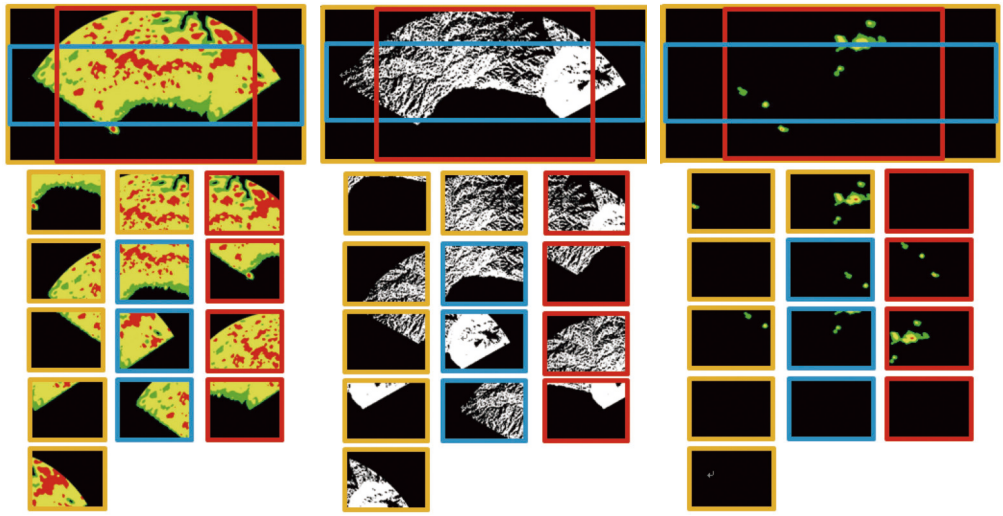

(a) RF images (b) DEM images (c) Label images

Fig. 6 The cropped images

3.2 The proposed DCNN

3.2.1 Network architecture

Inspired by ResNet [10], ENet [32] and SegNet [33], the proposed CNN architecture is depicted in Fig. 7, which is composed of one initial block, five stages, and one full convolutional (conv.) layer. In the initial block, there are a convolution with 13 filters and a Max pooling (pool.) layer. Their feature maps are concatenated together. Stage 1−3 complete the encode processing, while the decoder is comprised of Stage 4 and Stage 5. Stages 1−3 contain five different bottleneck modules, while Stage 4 and Stage 5 consist of three different bottleneck modules. Finally, the previous generated features are embedded into a feature space in a bare fully connected (FC) layer as the last module of the network, which alone takes up a sizeable portion of the decoder processing time.

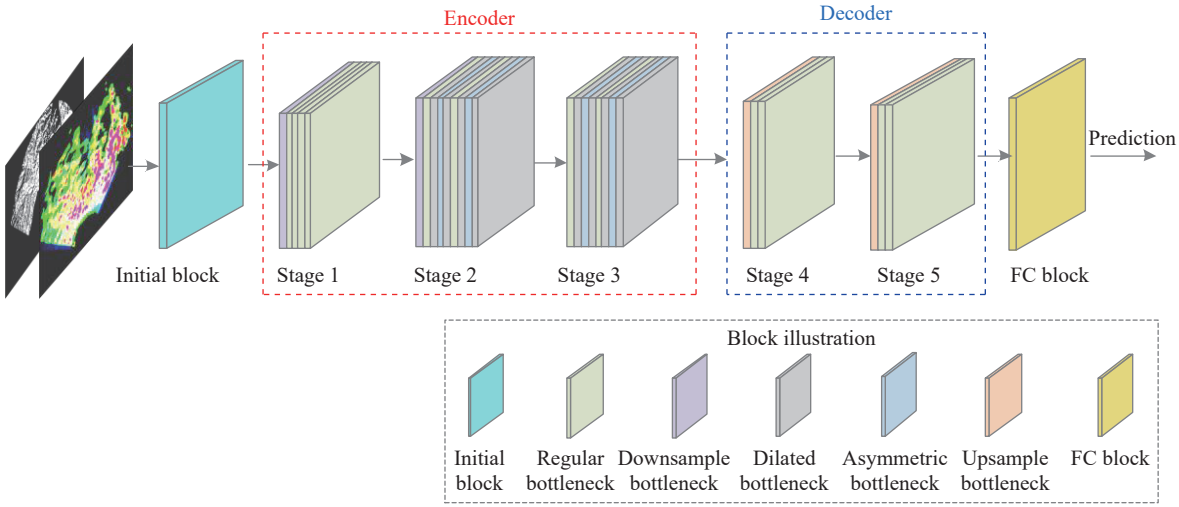

Fig. 7 Our proposed DCNN architecture

As shown in Fig. 7 and Fig. 8, bottleneck modules can be regular, dilated, asymmetric, down-sampling, and up-sampling. For regular bottleneck in light green, there are three conv. layers: a 1×1 projection that reduces the dimensionality, a main 3×3 conv. layer, and a 1×1 expansion. We place batch normalization (norm.) [34] and parameter rectified linear unit (PReLU) [35] between all conv., and spatial dropout [36] at the end of conv. branches, as shown in the left of Fig. 8 before addition. For dilated bottleneck in gray, the dilated conv. [24] is employed to replace the main conv. layer of regular bottleneck to avoid overly down-sampling the feature maps,

and also have a wide receptive field. For the down-sampling bottleneck in light purple, a 2×2 Max pool. layer is complemented to the left main branch and the 1×1 projection of regular bottleneck is modified as a 2×2 conv. layer. For the up-sampling bottleneck in light brown, a 1×1 conv. layer, a Batch norm. layer and a Max unpool. layer are complemented to the branch together, in the right before the addition. For the asymmetric bottleneck, the main conv. of regular bottleneck is replaced with two asymmetric convolution operators. Herein, we set a 3×3 conv. as an example, which can be decomposed of a sequence of 3×1 and 1×3 conv. operators.

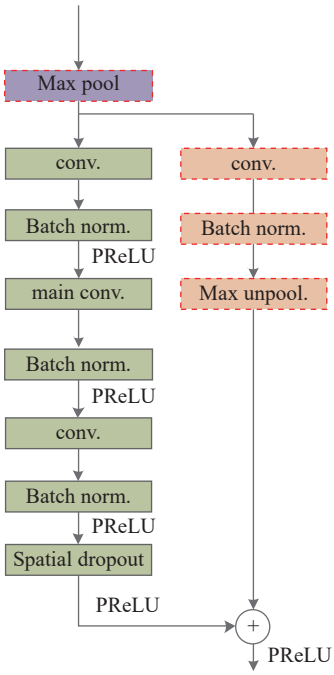

Fig. 8 Bottleneck module

It is shown that our proposed network mainly performs in two stages: first the encoder is only trained to categorize down-sampled regions of the input images, and then we append the decoder and train the network to perform up-sampling and pixel-wise classification. Similar to SegNet [33], the semantic segmentation of input image completes the down-sampling by saving indices of elements chosen in Max pool. layers and using them to produce sparse up-sampled maps in the decoder. Many input samples are fed to the network for training, which is regarded as an iterative process that progresses neurons during the forward pass, and updates the network parameters during the backward pass until the calculated loss is minimized. Then the trained network with optimized parameters (e.g., the conv. layers' weights) is employed to classify the meteorology targets, meanwhile the classified ground clutters would be suppressed.

3.2.2 Forward pass feature extraction

In the forward pass progress, the features are extracted in each network layer, followed with convolutions. The conv. layer convolves feature maps with a set of learnable filters, which can transform the previous input feature space into appropriate codes of representation. These filters are randomly initialized with Gaussian noise. After the convolution processing, the output feature map can be depicted as

$$\boldsymbol{\beta}_j^q=\sigma\left(\sum_{j=1}^{m_c}\boldsymbol{x}_h^{(q-1)}*\boldsymbol{w}_{jh}^q+b_j^q\right) \tag{3}$$

where $\boldsymbol{\beta}_j^q$ refers to the jth feature map of the qth layer, $\boldsymbol{x}_h^{(q-1)}$ is the hth input feature map of the $(q-1)$th layer, m_c is the number of fed feature maps, $\boldsymbol{w}_{jh}^q$ and b_j^q represent the filters and biases to be trained in the qth layer, respectively. $\sigma(\cdot)$ is the nonlinear activation function. $*$ denotes the convolution operation. For the goal of learning the negative slope of non-linearity, the PReLU [35] is employed to replace the traditional ReLU as the activation function, and is given by

$$\boldsymbol{\beta}_j^q=\begin{cases}\displaystyle\sum_{j=1}^{m_c}\boldsymbol{x}_h^{(q-1)}*\boldsymbol{w}_{jh}^q+b_j^q, & \displaystyle\sum_{j=1}^{m_c}\boldsymbol{x}_h^{(q-1)}*\boldsymbol{w}_{jh}^q+b_j^q>0\\ \displaystyle k\left(\sum_{j=1}^{m_c}\boldsymbol{x}_h^{(q-1)}*\boldsymbol{w}_{jh}^q+b_j^q\right), & \text{else}\end{cases} \tag{4}$$

where $0\leqslant k<1$ is an additional parameter. Especially, when $k=0$, PReLU is transformed to ReLU.

The Max pool. layer is designed to down-sample the feature maps and also keep the feature shifting, rotational and scaling invariance. The Max pool. operator computes the maximum response of the previous feature map in a window, which can be formulated as

$$\boldsymbol{\beta}_j^q(p,q)=\max_{0\leqslant u<\omega_1,0\leqslant v<\omega_2}\boldsymbol{\beta}_j^q(p+u,q+v) \tag{5}$$

where ω_1 and ω_2 are the pool. window sizes. That is the maximum neuron value in the pooling window is selected and others are disregarded. Meanwhile, overlapping and non-overlapping are two pool. tricks. In this work, we adopt the overlapping pool. operator.

In the FC layer, the previous generated features are embedded into a feature space for better separation of different classes. Let the input of FC layer be a vector $\boldsymbol{x}^{(q-1)}$, whose dimension is m_f, then the output is expressed as

$$\boldsymbol{\beta}_j^q=\sigma\left(\sum_{j=1}^{mg}\boldsymbol{x}_h^{(q-1)}+\boldsymbol{w}_{jh}^q+b_j^q\right) \tag{6}$$

where $\boldsymbol{\beta}_j^q$ is the jth output unit of the qth FC layer, $\boldsymbol{x}_h^{(q-1)}$ is the hth element of $\boldsymbol{x}^{(q-1)}$, $\boldsymbol{w}_{jh}^q$ and b_j^q constitute the

trainable parameters. A spatial dropout method is used to sparse the neurons and avoid over-fitting [36].

3.2.3 Backward pass network optimization

To obtain the excepted convergence effects of the trained network, Softmax function is used to calculate the error between the predicted results and the actual input labels. The error can be employed to update the network parameters during the backward pass. Then the weights $\boldsymbol{w}_{jh}^{q}$ and biases b_j^q can be optimized quickly. In this work, the binary cross entropy (BCE) loss function is used as the loss function. To simplify the parameter notation, let $\boldsymbol{\Theta}$ denote the parameter combination of the whole network, including the weights and biases. $F_{\boldsymbol{\Theta}}$ is represented as the nonlinear transformation with $\boldsymbol{\Theta}$. Then the BCE loss function is given by

$$E(F_{\boldsymbol{\Theta}}|\boldsymbol{S},\boldsymbol{Y}) = -\frac{1}{N_l}\sum_{i=1}^{N_l}\left(\boldsymbol{y}_i^{\mathrm{T}}\ln \boldsymbol{s}_i + \left(1-\boldsymbol{y}_i^{\mathrm{T}}\right)\ln(1-\boldsymbol{s}_i)\right) \quad (7)$$

where $\boldsymbol{S}=[\boldsymbol{s}_1,\boldsymbol{s}_2,\cdots,\boldsymbol{s}_{N_l}]$ is the input training samples, $\boldsymbol{Y}=[\boldsymbol{y}_1,\boldsymbol{y}_2,\cdots,\boldsymbol{y}_{N_l}]$ is the corresponding label vector. Adaptive moment estimation (Adam) algorithm with mini-batch [18] is adopted to optimize the BCE loss function and learn the network parameters $\boldsymbol{\Theta}$ in $F_{\boldsymbol{\Theta}}$. Suppose that the parameter vector of the tth iteration is $\boldsymbol{\Theta}_t$, then the parameter vector of the (t+1)th iteration is updated as

$$\boldsymbol{\Theta}_{t+1} = \boldsymbol{\Theta}_t - \mu\frac{\partial E(F_{\boldsymbol{\Theta}}|\boldsymbol{S},\boldsymbol{Y})}{\partial \boldsymbol{\Theta}} \quad (8)$$

where μ is the learning rate, $\dfrac{\partial E(F_{\boldsymbol{\Theta}}|\boldsymbol{S},\boldsymbol{Y})}{\partial \boldsymbol{\Theta}}$ represents the change rate of network parameter vector.

4. Experiments and analysis

In this section, the proposed method is evaluated quantitatively and qualitatively on actually measured meteorology echo of airborne weather radar. We first introduce experimental data and training strategy in Subsection 4.1. Then, evaluation factors are depicted in Subsection 4.2. The effectiveness of the proposed network is demonstrated by comparisons with another two methods in Subsection 4.3. The counterparts include the traditional FCN [18] and SegNet [27]. In Subsection 4.4, we also evaluate the effects of parameter setting on network performances.

4.1 Experimental data and training strategy

Followed with cropping processing, the input image size (as shown in Fig. 5) is 480×360. For the sake of concise exhibition, the normalized reflectance of meteorological targets can be divided into four classes, according to three thresholds given by $t_1=0.14$, $t_2=0.5$, and $t_3=0.7$. When the transmitted ground is a mountain with larger height in DEM images, the calculated RF would be larger with red. A total of 12 740 cropped images are obtained, which are divided into two datasets in a ratio of 8:2 for training and testing, respectively.

As depicted in Table 1, to train the network effectively, an adaptive moment estimation optimizer is used with the initial learning rate $\mu=0.000\,5$, which declines 90% every 100 epochs. A total of 300 epochs are implemented with batch size equalling to 10. Empirically, the parameter k of PReLU is set to 0.25 and the optimizer parameters (β_1,β_2) are 0.9 and 0.999. The total parameter number and the flops of our proposed network are 360 K and 3.5 G, respectively.

Table 1 Parameter configuration of our training network

Parameter	Value
Learning rate μ	0.000 5
Decline factor of learning rate	0.1
Epoch	300
k of PReLU in (4)	0.25
Batch size	10
Optimizer parameter (β_1, β_2)	(0.9, 0.999)

4.2 Evaluation factors

The confusion matrix is employed to statistically analyse the performances of the trained CNN model. Pixels in label images and predict results are divided into foreground and background by a threshold equalling to 0.14. The foreground contains the actual meteorology targets and is considered positive, while the background is considered negative. Thus the correctly classified pixels are categorized in true positive (TP) and true negative (TN), and the misclassified test images are denoted in false positive (FP) and false negative (FN). The classified performances are evaluated by the precision, probability of detection (POD), false alarm ratio (FAR) and critical success index (CSI), which are calculated as

$$\text{Precision} = \frac{\text{TP}}{\text{TP}+\text{FP}}, \quad (9)$$

$$\text{POD} = \frac{\text{TP}}{\text{TP}+\text{FN}} = \text{recall}, \quad (10)$$

$$\text{FAR} = \frac{\text{FP}}{\text{TP}+\text{FP}} = 1-\text{precision}, \quad (11)$$

$$\text{CSI} = \frac{\text{TP}}{\text{TP}+\text{FP}+\text{FN}}. \quad (12)$$

In addition, let the expected output image and the actual output image be denoted as $\boldsymbol{I}$ and $\boldsymbol{I}^p$, and the corresponding pixels at position (i, j) are written as $\text{pixel}_{i,j}$

and $\text{pixel}_{i,j}^{P}$. Then, the intersection of union (IOU) and image correlation are also adopted as evaluation indicators:

$$\text{IOU} = \frac{\boldsymbol{I} \cap \boldsymbol{I}^{p}}{\boldsymbol{I} \cup \boldsymbol{I}^{p}}, \tag{13}$$

$$\text{Corr} = \frac{\sum_{i,j}\left(\text{pixel}_{i,j}^{P} \cdot \text{pixel}_{i,j}\right)}{\sqrt{\sum_{i,j}\left(\text{pixel}_{i,j}^{P}\right)^{2} \cdot \sum_{i,j}\left(\text{pixel}_{i,j}\right)^{2}}}, \tag{14}$$

where $\cap$ and $\cup$ represent the intersection and union operators, respectively. It is illustrated that if the evaluation only considers POD, the trained model may over-predict the meteorological targets. If the evaluation consider only FAR, the model may under-predict the ground clutter. Especially, the perfect model would have POD=1, FRA=0, CSI=1, Corr=1, and IOU=1 based on the label measures.

4.3 Results and comparisons

Table 2 and Table 3 show the evaluation results of counterparts in the training and testing stages. It is shown that the evaluation indicators of the proposed network are the best among the candidate networks. Herein, we set the testing results as an example. The precision achieves 0.88 and the CSI is 0.81. There are separately more than 0.2 improvements in comparison to those of SegNet [33]. FCN [22] achieves a high FAR (0.31), a low POD (0.56) and a low CSI (0.45), because more TP and TN are misclassified than other approaches. It is observed that the Corr (0.90) and IOU (0.41) indicators of the proposed network are the highest, which means that our network output images are closer to the final meteorology detection images (labels) after ground clutter suppression, comparing with other networks.

Table 2 Evaluation result comparisons in the training

Network	Precision	POD	FAR	CSI	Corr	IOU
FCN [18]	0.73	0.59	0.27	0.48	0.66	0.30
SegNet [27]	0.84	0.80	0.16	0.69	0.82	0.30
Our proposed network	0.89	0.96	0.11	0.86	0.93	0.43

Table 3 Evaluation result comparisons in the testing

Network	Precision	POD	FAR	CSI	Corr	IOU
FCN [18]	0.69	0.56	0.31	0.45	0.62	0.29
SegNet [27]	0.80	0.72	0.20	0.61	0.76	0.30
Our proposed network	0.88	0.91	0.12	0.81	0.90	0.41

In comparison to the architectures of FCN and SegNet, it is obvious that other different types of bottlenecks, except for the regular bottleneck, are designed to extract the image features in different stages of the proposed DCNN, such as the dilated bottleneck and asymmetric bottleneck. Benefiting from the unique bottleneck modules, our proposed DCNN has a better ability to capture the feature differences between the actual meteorology targets and clutters from the DEM images and weather radar images.

With the above cropped criterion and sub-image index, the output cropped images can be spliced together. Fig. 9 is the meteorology detection result of the proposed network, where the input is Fig. 2 and Fig. 4, and the corresponding label is Fig. 5. Fig. 10 is another typical network-based meteorology detection result. As shown in Fig. 5, Fig. 11, and Fig. 12, the high intensity areas in yellow and red are well preserved in terms of their size and texture details by using the proposed approach.

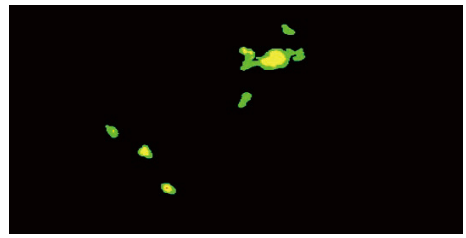

Fig. 9 DCNN-based meteorology detection result, in comparison to the label in Fig. 5

(a) Final meteorology detection result of airborne weather radar (i.e., the label)

(b) The proposed network's output

Fig. 10 Another typical meteorology detection comparison

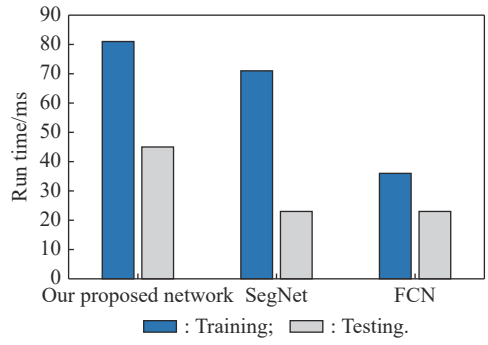

Fig. 11 Runtime comparisons of different counterparts

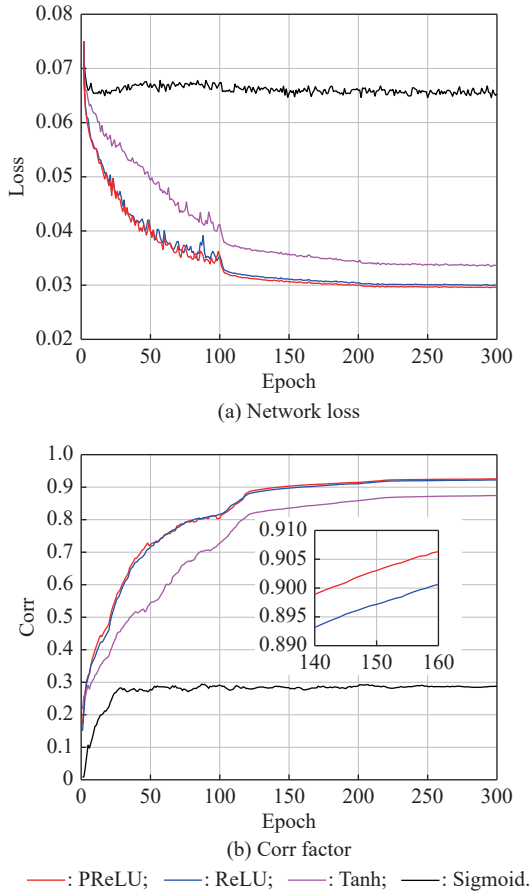

Fig. 12 Network loss and Corr factor comparisons with different activation functions

All the experiments are implemented in the python environment on a Dell T7910 workstation with TITAN RTX GPU and 128 GB memory. Fig. 11 shows the training and testing runtime of different counterparts on the same datasets. Due to more network layers and fine feature extraction processing, our proposed network consumes more runtime. However, there are more obvious advantages on the evaluators as shown in Table 2 and Table 3.

4.4 Analysis of network parameter setting

To validate the feasibility and effectiveness, we also carry out two different comparison experiments. The proposed network with different activation functions and lapping function are further evaluated, respectively.

4.4.1 Evaluation of activation function

In this subsection, the performances of our trained network with different activation functions are evaluated and compared. PReLU, ReLU, sigmoid, and tanh activation functions are adopted in (3), respectively. The loss and Corr factor comparisons are shown in Fig. 12. It can be observed that models trained with PReLU and ReLU perform better than others. The trained network loss with PReLU is the smallest and the Corr factor is the largest. Especially, when the epoch number is more than 150, the loss is about 0.03 and the Corr factor is about 0.9.

4.4.2 Evaluation of overlapping and non-overlapping pooling

We also compare the performances of the trained network with overlapping and non-overlapping pooling, where PReLU is employed. The results are shown in Fig. 13 and we can find that the use of the overlapping pooling operation results in better performances. The trick of overlapping pooling is adopted in the proposed network.

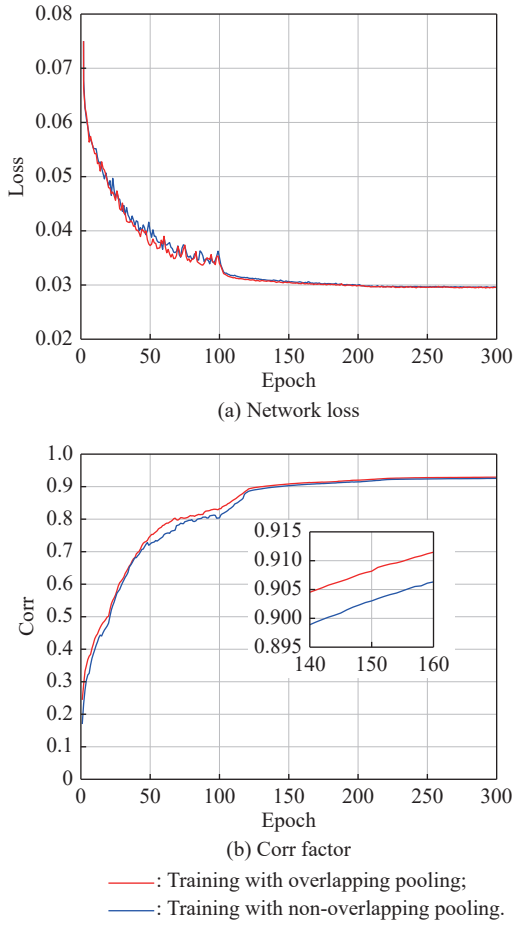

Fig. 13 Network loss and Corr factor comparisons with overlapping and non-overlapping operation

5. Conclusions

In this work, a DCNN for meteorology target detection in airborne weather radar images is designed and evaluated. For each weather radar image, the corresponding DEM

image with the same spatial domain is obtained and also employed to train the DCNN together for the meteorology target detection and ground clutter suppression. In each bottleneck module of DCNN, the features of airborne radar images and DEM images are learned based on conv., norm., pool./unpool. and dropout processing. Comprehensive evaluations of our proposed network are provided based on actually measured airborne weather radar images and DEM images. The experimental results show that our proposed DCNN outperform the conventional FCN and SegNet methods in terms of six evaluation factors. It demonstrates the feasibility and effectiveness of DL in the meteorology detection application of weather radar. The proposed DCNN can also be employed to detect other types of meteorology without minimal efforts on network variables or parameter changes.

Future research may be directed in two directions. The optimization and acceleration algorithm of the proposed model is first planned to develop. Meanwhile, the exploration of additional meteorological elements is considered further to make the prediction model more accurate.

References

[1] WANG H J, SHAO N, RAN Y B. Identification of precipitation-clouds based on the dual-polarization Doppler weather radar echoes using deep-learning method. IEEE Access, 2019, 7: 12822–12831.

[2] HAN L, SUN J Z, ZHANG W. Convolutional neural network for convective storm nowcasting using 3-D Doppler weather radar data. IEEE Trans. on Geoscience and Remote Sensing, 2020, 58(2): 1487–1495.

[3] GUANG Y, ZONG X L, XU F G. Prediction of weather radar images via a deep LSTM for nowcasting. Proc. of the International Joint Conference on Neural Networks, 2020. DOI: 10.1109/IJCNN48605.2020.9206889.

[4] GURUNG I, PENG C, MASKEY M. Deep feature extraction and its application for hailstorm detection in a large collection of radar images. Signal, Image and Video Processing, 2019, 13: 541–549.

[5] YANG H Y, WANG F Y. Meteorological radar noise image semantic segmentation method based on deep convolutional neural network. Journal of Electronics and Information Technology, 2019, 41(10): 2373–2381.

[6] SZEGEDY C, VANHOUCKE V, LOFFE S. Rethinking the inception architecture for computer vision. Proc. of the IEEE Conference on Computer Vision and Pattern Recognition, 2016: 2818−2826.

[7] PRADHAN R, AYGUN R, MASKEY M. Tropical cyclone intensity estimation using a deep convolutional neural network. IEEE Trans. on Image Processing, 2018, 27(2): 692–702.

[8] TRAN Q K, SONG S K. Computer vision in precipitation nowcasting: applying image quality assessment metrics for training deep neural networks. Atmosphere, 2019, 10: 244.

[9] KRIZHEVSKY A, SUTSKEVER I, HINTON G E. ImageNet classification with deep convolutional neural networks. Communications of ACM, 2017, 60: 84–90.

[10] HE K M, ZHANG X Y, REN S Q. Deep residual learning for image recognition. Proc. of the IEEE Conference on Computer Vision and Pattern Recognition, 2016: 770−778.

[11] XIONG W, LUO J S, YU C P. Power line detection in millimeter-wave radar images applying convolutional neural networks. IET Radar, Sonar and Navigation, 2021, 15(9): 1083–1095.

[12] NIU S R, QIU X L, LEI B. Parameter extraction based on deep neural network for SAR target simulation. IEEE Trans. on Geoscience and Remote Sensing, 2020, 58(7): 4901–4914.

[13] DENG Z P, SUN H, ZHOU S L. Learning deep ship detector in SAR images from scratch. IEEE Trans. on Geoscience and Remote Sensing, 2019, 57(6): 4021–4039.

[14] ZHOU L, WEI S Y, CUI Z M. Multi objective detection of complex background radar image based on deep learning. Systems Engineering and Electronics, 2019, 41(6): 1258–1264. (in Chinese)

[15] SHI S N, DONG Z Y, YANG J. Sea-surface small target detection based on autonomic learning of time-frequency graph. Systems Engineering and Electronics, 2021, 43(1): 33–41. (in Chinese)

[16] TAO Y, GAO X, HSU K. A two-stage deep neural network framework for precipitation estimation from Bispectral satellite information. Hydrometeorology, 2018, 19(2): 393–408.

[17] NI X, LIU C T, CECIL D J. On the detection of hail using satellite passive microwave radiometers and precipitation radar. Applied Meteorology and Climate, 2017, 56(10): 2693–2709.

[18] WANG H J, RAN Y B, DENG Y Y. Study on deep-learning-based identification of hydrometeors observed by dual polarization Doppler weather radars. EURASIP Journal on Wireless Communication Networking, 2017, 2017: 173.

[19] TAO Y M, GAO X G, IHLER A. Precipitation identification with bispectral satellite information using deep learning approaches. Hydrometeorology, 2017, 18(5): 1271–1283.

[20] HAM Y G, KIM J H, LUO J J. Deep learning for multi-year ENSO forecasts. Nature, 2019, 573: 568–572.

[21] RAVURI S, LENC K, WILLSON M. Skilful precipitation nowcasting using deep generative models of radar. Nature, 2021, 597: 672–677.

[22] SHELHAMER E, LONG J, DARRELL T. Fully convolutional networks for semantic segmentation. IEEE Trans. on Pattern Analysis and Machine Intelligence, 2017, 39(4): 640–651.

[23] LI F X, LONG Z R, HE P. Fully convolutional pyramidal networks for semantic segmentation. IEEE Access, 2020, 8: 229132–229140.

[24] CHEN L C, PAPANDREOU G, KOKKINOS I. DeepLab: semantic image segmentation with deep convolutional nets, atrous convolution, and fully connected CRFs. IEEE Trans. on Pattern Analysis and Machine Intelligence, 2018, 40(4): 834–848.

[25] DONG C, JU Y W. Ship object detection SAR images based on semantic segmentation. Systems Engineering and Electronics, 2022, 44(4): 1195–1201. (in Chinese)

[26] LIU Z Y, XIE C S, LI J J. Smoke region segmentation recognition algorithm based on improved Deeplabv3+. Systems Engineering and Electronics, 2021, 43(2): 328–335. (in Chinese)

[27] LECUN Y, BENGIO Y, HINTON G. Deep learning. Nature, 2015, 521: 436–444.

[28] SCHMIDHUBER J. Deep learning in neural networks: an overview. Neural Networks, 2014, 61: 85–117.
[29] SKOLNIK M I. Radar handbook. 3rd ed. New York: McGraw-Hill Press, 2008.
[30] KUREKIN A, RADFORD D, LEVER K. New method for generating site-specific clutter map for land-based radar by using multimodal remote-sensing images and digital terrain data. IET Radar, Sonar and Navigation, 2011, 5: 374–388.
[31] KUREKIN A, SHARK L K, LEVER K. Site-specific land clutter modelling based on radar remote sensing images and digital terrain data. Proc. of the IEEE Conference on Image and Signal Processing for Remote Sensing XVI, 2010: 25−36.
[32] PASZKE A, CHAURASIA A, KIM S. ENet: a deep neural network architecture for real-time semantic segmentation. https://arxiv.org/pdf/1606.02147.pdf.
[33] BADRINARAYANAN V, KENDALL A, CIPOLLA R. Segnet: a deep convolutional encoder-decoder architecture for image segmentation. IEEE Trans. on Pattern Analysis and Machine Intelligence, 2017, 39(12): 2481–2495.
[34] IOFFE S, SZEGEDY C. Batch normalization: accelerating deep network training by reducing internal covariate shift. Proc. of the International Conference on Machine Learning, 2015: 448−456.
[35] HE K M, ZHANG X Y, REN S Q. Delving deep into rectifiers: surpassing human-level performance on imagenet classification. Proc. of the IEEE International Conference on Computer Vision, 2015: 1026−1034.
[36] ACHILLE A, SOATTO S. Information dropout: learning optimal representations through noisy computation. IEEE Trans. on Pattern Analysis and Machine Intelligence, 2018, 40(12): 2897–2905.

Biographies

YU Chaopeng was born in 1977. He is now a researcher-level senior engineer in Aviation Industry Corporation of China (AVIC) Leihua Electronic Technology Institute. His research interests are airborne radar system and flight environment integrated surveillance system (ISS).
E-mail: yuchaopeng@raa.org.cn

XIONG Wei was born in 1984. He received his Ph.D. degree from School of Electronic and Information Engineering, Nanjing University of Aeronautics and Astronautics. Supported by China Scholarship Council (CSC), he studied abroad as a visiting scholar in the Department of Communication at the University of Pisa in Italy from October 2016 to September 2017. He is now a senior engineer in Aviation Industry Corporation of China Leihua Electronic Technology Institute. His research interests are airborne meteorological anti-collision radar system and integrated collision avoidance system of flight environment.
E-mail: xiongweiwhumath@sina.com

LI Xiaoqing was born in 1995. He received his B.S. degree from Xiangtan University in 2018 and M.S. degree from Beihang University in 2021. He is now an engineer in Aviation Industry Corporation of China Leihua Electronic Technology Institute. His research interests are radar target recognition and signal processing.
E-mail: 1032332623@qq.com

DONG Lei was born in 1983. He received his B.S. and M.S. degrees from Jiangsu University, in 2005 and 2008, respectively, and Ph.D. degree from Beihang University, in 2013. Since 2013, he has been a teacher with the Airworthiness College, Civil Aviation University of China. He is currently an associate professor. His research interests include model-based systems engineering, model-based safety assessment, and integrated modular avionics system.
E-mail: dlcauc@126.com